SCIENCE CHINA
Information Sciences

June 2023, Vol. 66 160403:1–160403:17
https://doi.org/10.1007/s11432-023-3753-9

• REVIEW •
Special Topic: Two-Dimensional Materials and Device Applications

Multidimensional modulation of light fields via a combination of two-dimensional materials and meta-structures

Zhipeng ZHENG†, Yijing HUANG†, Feng WU†, Han ZHANG & Zheyu FANG*

School of Physics, State Key Laboratory for Mesoscopic Physics, Academy for Advanced Interdisciplinary Studies, Collaborative Innovation Center of Quantum Matter, Nano-optoelectronics Frontier Center of Ministry of Education, Peking University, Beijing 100871*, China*

Received 14 March 2023/Revised 6 April 2023/Accepted 24 April 2023/Published online 19 May 2023

Abstract In recent years, researchers have increasingly directed their attention towards modulating light fields through the unique properties of two-dimensional materials and the free designability of meta-structures. Graphene, transition metal sulfides, transition metal nitrides, and other two-dimensional materials have emerged as star materials in recent years due to their extraordinary properties that are vastly different from those of traditional three-dimensional materials. As a result, these materials hold immense potential for further exploration and research. Taking advantage of the free designability of meta-structures can be an effective means of unlocking the full potential of 2D materials. Accordingly, this review presents an overview of recent research progress in the area of light field modulation achieved by combining 2D materials with meta-structures. The review initially covers the properties of 2D materials, followed by the concepts, principles, design, and preparation of meta-structures. Then the review delves into the concrete examples of the impact and effect of the combination on light field modulation. Lastly, the review concludes with a comprehensive summary and analysis of the current challenges and potential future developments of combining 2D materials with meta-structures.

Keywords two-dimensional materials, electromagnetic meta-structures, light field modulation, surface plasma polarisation, surface plasmon

Citation Zheng Z P, Huang Y J, Wu F, et al. Multidimensional modulation of light fields via a combination of two-dimensional materials and meta-structures. Sci China Inf Sci, 2023, 66(6): 160403, https://doi.org/10.1007/s11432-023-3753-9

1 Introduction

In recent years, both domestic and foreign researchers have explored various approaches and perspectives to regulate electromagnetic waves [1–4]. There are many parameters of electromagnetic waves that need to be regulated, including amplitude, phase, polarization state, frequency, and orbital angular momentum, as shown in Figure 1. Correspondingly, there are a number of functions that can be achieved by modulating electromagnetic waves, such as switching, modulation, and filtering [5–8]. Diverse regulation of electromagnetic waves can be achieved by establishing new technologies, exploring new materials, designing new structures, and creating new devices, which can be applied to various fields based on electromagnetic wave technology, such as imaging, sensing, and communication [9–11].

In the field of research on the modulation of electromagnetic waves through new materials and structures, there are two promising paths. One approach to achieve electromagnetic wave modulation in a specific frequency band is by exploiting the distinctive properties of emerging two-dimensional materials, such as graphene, transition metal sulfides, transition metal nitrides, and others [12–14]. The exotic properties that have garnered significant attention include high-temperature superconductivity, magic angles in graphene, chirality, and others [15–17]. Another approach that is known for its high degree of

* Corresponding author (email: zhyfang@pku.edu.cn)
† Zheng Z P, Huang Y J, and Wu F have the same contribution to this work.

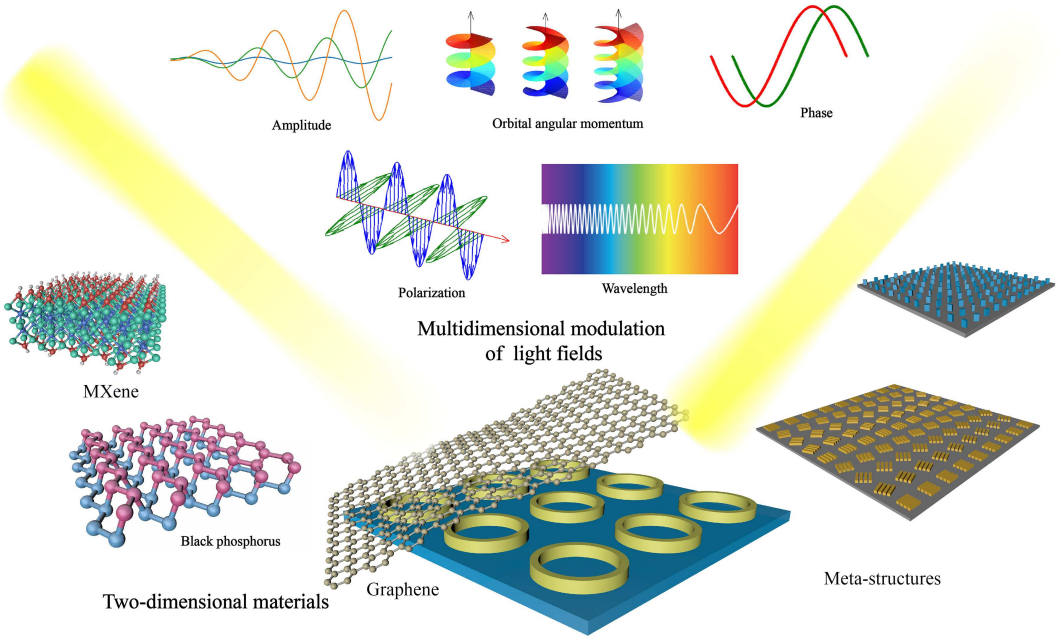

Figure 1 (Color online) Schematic representation of multidimensional modulation of light fields via a combination of two-dimensional materials and meta-structures.

design freedom to achieve directional modulation of electromagnetic waves is through the construction of artificial meta-structures that deviate from the natural materials' original properties [18–20]. Both 2D materials and meta-structures can modulate light fields to a certain extent, but with a different focus, the former relies mainly on the inherent properties of the material, while the latter relies on the properties of the designed structure [20–23]. The different focus of these two approaches results in different modulations of electromagnetic waves, each with its own strengths and weaknesses. Therefore, it is a valuable research topic to investigate how to complement their strengths and weaknesses to achieve a more comprehensive influence and control of electromagnetic waves. Besides, the preparation processes for both 2D materials and meta-structures are gradually being improved, which will help reduce the obstacles to their practical applications [24–28].

This paper provides a review of the modulation of electromagnetic waves from the perspectives of new materials and new structures. In the main text, we first introduce the properties of several representative two-dimensional materials, such as graphene, transition metal sulfides, and transition metal nitrides. We then provide a brief introduction to the concept of meta-structures, including the principles of light field modulation, design methods, and several important processes involved in the processing and fabrication of meta-structures. Next, analysis and discussion are presented on the effects of combining these three representative 2D materials with meta-structures, providing specific case studies as illustrations. Finally, the current challenges and potential future developments of integrating 2D materials with meta-structures are summarized and analyzed.

2 Two-dimensional materials

2.1 Graphene

Geim, Novoselov, and their collaborators published the first report on electric field effects in single-crystal graphite films (that is, graphene) in 2004, setting off a wave of graphene research [29]. Graphene exhibits good properties in terms of mechanics, heat, and optoelectronics, such as high elastic modulus, high electron mobility at room temperature, and good electrical conductivity, and is gradually being used in biomedicine, optoelectronic regulation, and other fields [30–34]. Single-layer graphene (SLG) has a honeycomb lattice structure composed of carbon atoms arranged in a hexagonal structure. Graphene has good stability due to larger π bonds and sp^2 hybridization between carbon atoms. There are six Dirac points in the first Brillouin zone. The conduction and valence bands are conical around the Dirac point

and are symmetric about the Dirac point, so electrons and holes are the same in pure graphene. It hints at the nature of the metal. In particular, the energy band of graphene is zero.

The interaction between graphene itself and electromagnetic waves is not strong. The light transmittance in the terahertz frequency band has reached more than 97.7%, and the absorption rate in the visible and infrared bands is only 2.3%, which is transparent. Therefore, single-layer pure graphene has limited control over electromagnetic waves. Although graphene is a good electrical conductor, due to its single-atom thickness, its surface impedance is relatively large compared to metal in microwave and millimeter wave bands [34]. Graphene can excite surface plasmons in the infrared band, so it has broad prospects for detection and imaging in the infrared band.

In order to strengthen the interaction between electromagnetic waves and graphene, graphene is often prepared into a specific structure, such as periodic doping of graphene, or prepared into stacks, crosses, discs, to form a resonance structure. Of course, by changing the chemical potential of graphene to change its electrical conductivity [35], its response to electromagnetic waves can also be changed. Using the above method, we can use graphene to assist in the regulation of electromagnetic waves. Combining graphene with a metasurface and making full use of the electromagnetic properties of graphene can achieve the regulation of the phase, amplitude, and polarization state of electromagnetic waves.

The modulation of electromagnetic waves by graphene can be realized by the plasmons generated on its surface after the irradiation of electromagnetic waves. Plasmons are high-frequency collective density oscillations ubiquitous in e-liquids and present in many metals and semiconductors. In the visible light band, plasmons can exist at the intersection interface of metal and dielectric, and electromagnetic waves are mainly distributed in a small range at the interface. Using this characteristic at the interface can realize the regulation of electromagnetic waves and produce many practical applications, but due to the characteristics of the metal itself, loss and weak confinement in the terahertz and mid-infrared bands make its application difficult. On the contrary, graphene does not have the above-mentioned problems when generating plasmons on the surface in the terahertz and infrared bands. Therefore, it is necessary and promising to study graphene surface plasmons as a supplement to metal dielectrics [36]. Using scanning near-field optical microscopy can directly emit and image graphene plasmons. Using infrared nanoimaging, Fei et al. [37] found that the common graphene/SiO_2/Si back-gate structure supports propagating surface plasmons, as shown in Figures 2(a)–(e). Graphene plasmons have a wavelength of about 200 nm, at technologically relevant infrared frequencies they can travel several times this distance.

Graphene plasmons have many advantages. On the one hand, it localizes the electromagnetic field on the surface with only atomic thickness, showing strong field confinement. On the other hand, it shows great adjustability in optical response, which can pass through gate control, doping, chemical means, and traditional noble metal-based plasma modification [38]. Brar et al. [39] used infrared microscopy to observe the modes of tunable plasmonic graphene nanoresonator arrays as small as 15 nm, and calculations showed that the confined plasmonic modes have a localized optical density of states more than 10^6 larger than that of free space. The team also measured the resonant frequency as a function of the width of the nanoresonator, as shown in Figure 2(f) for the wave-vector-dependent dispersion relationship of graphene plasmons at mid-infrared energies. By changing the width of the nanoresonator and the carrier density of graphene, the frequency and intensity of plasmons can be adjusted, indicating that it has great tunable properties. Yan et al. [40] observed the direct interaction between localized graphene plasmons and infrared light using graphene microdisks, and the plasmons can be tuned by changing the disk diameter, disk filling number, filling number, and gating, as shown in Figure 2(g). Ju et al. [41] graphene microstrips successfully achieved plasmon excitation in the terahertz band, and graphene plasmon resonance can be tuned over a wide frequency range by changing the strip width and in-situ back gate, as shown in Figure 2(h).

2.2 TMDS

TMDS refers to transition metal dichalcogenides. Common representatives include MoS_2, WS_2, $MoSe_2$, and WSe_2. Although the properties of different material compositions are different, their physical properties are similar. The crystal structure and electronic structure of TMDS determine its various properties [42]. TMDS has T-phase and H-phase modes, as shown in Figures 3(a) and (b), in which the blue spheres represent transition metals, and the pink spheres represent S-group elements. The T-phase belongs to the octahedral structure, and the H-phase can be obtained after the chalcogen elements in the upper layer are rotated by 180°, which belongs to the triangular prism structure. TMDS can form

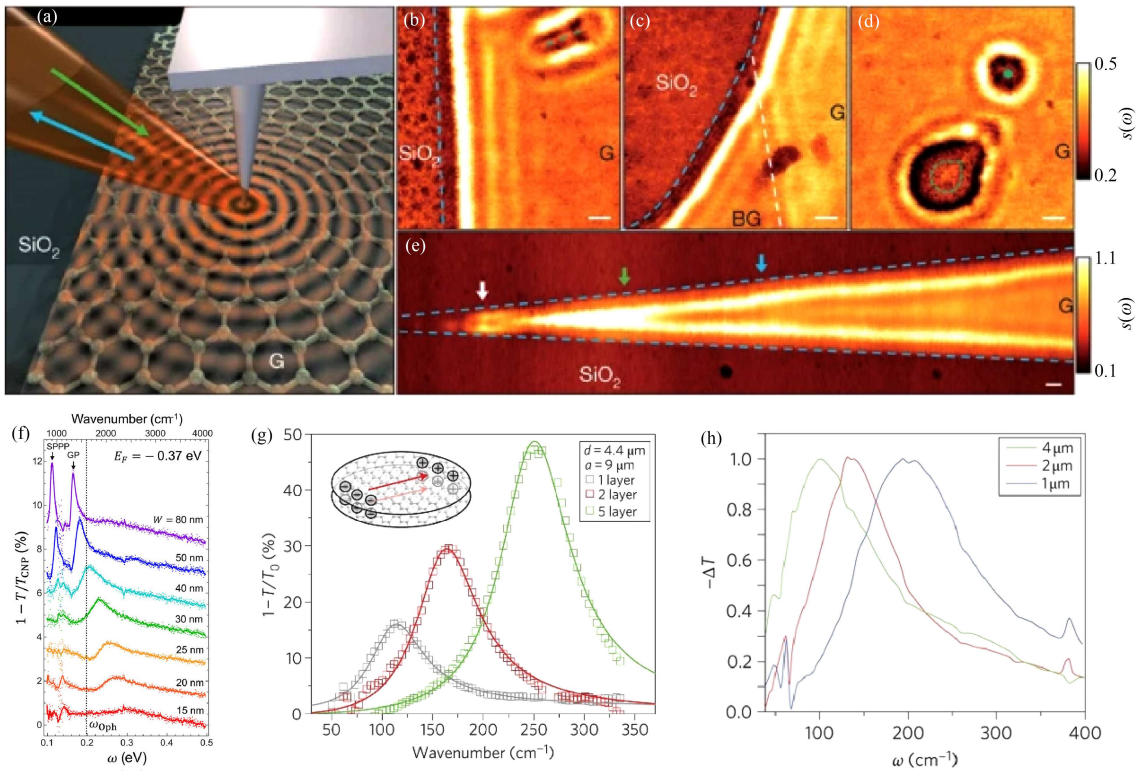

Figure 2 (Color online) (a) Infrared nanoimaging experiment diagram of graphene surface on SiO_2. Concentric red circles show plasma waves emitted by the glowing tip [37]. (b)–(e) Characteristic interference patterns near graphene edges (dashed blue lines) and defects (dashed green lines and green dots) and the boundary between monolayer and bilayer graphene (dashed white lines). Boundary and defect locations determined from AFM topography acquired simultaneously with near-field data [37] Copyright 2012 Nature Publishing Group. (f) Light transmission $E_F = -0.37$ eV for nanoresonator widths from 15 to 80 nm [39] Copyright 2013 American Chemical Society. (g) Graphene transmission extinction when the number of layers is one layer, two layers, and five layers [40] Copyright 2012 Nature Publishing Group. (h) In the case of doping concentration of, different graphite microstrips transmission spectrum [41] Copyright 2011 Nature Publishing Group.

different crystal structures, namely 1T, 1T′, 1Td, 2H, and 3R.

TMDS is a semiconductor with a large band gap and medium carrier mobility, unlike graphene. For example, the band gap of a single layer of PtS_2 is 1.2 eV. Interestingly, the band gap of TMDS has a certain correlation with the number of layers, as the thickness changes from bulk to monolayer, the band gap of the material becomes smaller, and the metallic nature becomes semiconducting. For example, the bandgap of single-lay $PtSe_2$ is 1.3 eV, while the bandgap of bulk is 0 eV; the MoS_2 of the semiconductor 2H stacking method realizes the indirect bandgap at the K point to the direct bandgap in the process of reducing the number of layers to a single layer. TMDS realizes the transition from indirect to direct bandgap from multilayer to monolayer film, and the intensity of corresponding photoluminescence (PL) also increases rapidly. PL refers to the process in which a substance absorbs photons (or electromagnetic waves) and re-radiates photons (or electromagnetic waves). Due to the unique structure and functional characteristics of TMDS, it has great prospects in supercapacitors, hotspot applications, and optoelectronics.

Excitons are quasi-particles existing in monolayer TMDS, which are electrons and holes combined due to the Coulomb interaction force, and have a small Bohr radius and a large oscillator strength. Small Bohr radii lead to overlapping electron and hole wave functions, and thus, large oscillator strengths while strong exciton absorption. Large oscillator strengths lead to fast radiative decay. The exciton binding energy of TMDS is an order of magnitude larger than that of ordinary semiconductors. At room temperature, the exciton effect also dominates the optical properties of TMDS, so it is necessary to study the basic properties of excitons [43]. In two-dimensional TMDS, in addition to the two degrees of freedom of spin and charge, the energy valley, that is, the extreme point of the solid energy band, is the third degree of freedom. Due to the breaking of space inversion symmetry, the adjacent two valleys K and K′ are not degenerate. The K valley and the K′ valley absorb and emit left-handed and right-handed light of opposite handedness, respectively. However, the natural valley fluorescence signal intensity is relatively weak at room temperature, and the scattering between K valley and K′ valley is equivalent, which will

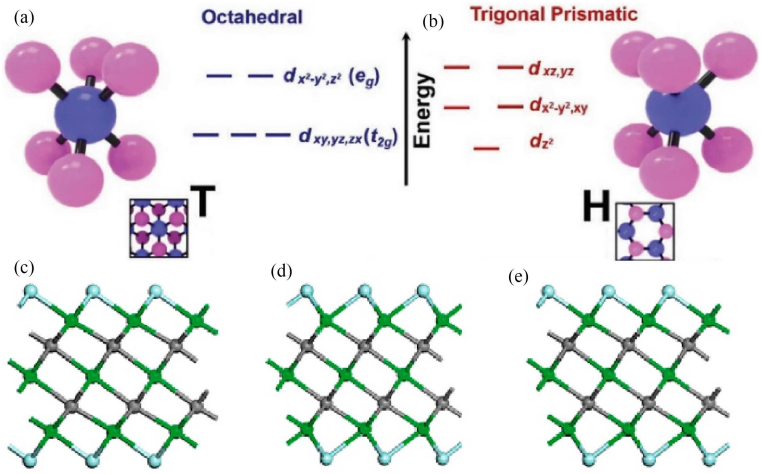

Figure 3 (Color online) Schematic diagram of the structure of TMDS and MXene (a) T-phase and (b) H-phase TMDS [42] Copyright 2021 Wiley-VCH GmbH. (c) I-$Ti_3C_2T_x$; (d) II-$Ti_3C_2T_x$; (e) III-$Ti_3C_2T_x$ [45] Copyright 2012 American Chemical Society.

limit its development and application [44]. In response to the above, the combination of TMDS and meta-structures is an effective way forward, as will be discussed in more detail later.

2.3 MXene

There are many functional groups on the surface of MXene. The general chemical formula is $M_{n+1}XT_n$, where M is a transition element metal, X is carbon or nitrogen, and T is a functional group, such as -OH, -F, and -O. MXene has a hexagonal crystal structure with a space group of $P36/mmc$.

MXene with consistent elemental composition and different structures can exhibit different properties. According to the distribution of functional groups, $Ti_3C_2T_x$ has three structures, as shown in Figure 3. There are two distributions of functional groups, the first is that the functional group is directly above the Ti, and the second is above the C atom on the same side. The I-$Ti_3C_2T_x$ has the first type on both sides, the II-$Ti_3C_2T_x$ has both sides of the second type, and III-$Ti_3C_2T_x$ has arbitrary functional group arrangements on both sides [45]. It is worth mentioning that more than one functional group can be present in a single substance [46].

Since the elements and functional groups constituting MXene can vary greatly, different MXene can exhibit different electronic properties. Through the precise control of the type and content of functional groups on the surface, it is possible to realize the leap from the conductor, semiconductor to insulator, and also realize the adjustment of its electrical conductivity [47], magnetic and optical properties. Taking the aforementioned $Ti_3C_2T_x$ as an example, due to the difference in surface functional groups, the band gaps of the first and third structures are 0.04 and 0.03 eV respectively, showing the performance of semiconductors; relatively speaking, the II-$Ti_3C_2T_x$ has a large number of electronic states near the Fermi level, showing the properties of metals. Reducing the functional groups on the surface of $Ti_3C_2T_x$ by calcination can directly increase its electrical conductivity by three times. Since the electrical conductivity and optical properties of MXene can be flexibly adjusted by precisely controlling the type and content of functional groups on the surface, it is easy to see that there will be more selectivity and freedom in the design of meta-structures using MXene.

2.4 Some other 2D materials

In addition to the several 2D materials mentioned above, there are other kinds of 2D materials, which we briefly introduce here. The massive black phosphorus has a direct bandgap with a value of about 0.31 eV at the Z point. Monolayer black phosphorus is also a direct gap semiconductor with high carrier mobility, its gap is 1.51 eV, and its relatively large band gap makes it advantageous [48]. Unlike graphene, monolayer black phosphorus exhibits in-plane anisotropy in optical properties and has excellent optical/phonon properties [49]. The properties of black phosphorus facilitate research into optoelectronics and novel electronics, such as logic transistors and broadband photodetectors [50].

Graphite carbonitride (g-C_3N_4) is a polymeric layered nanomaterial. g-C_3N_4 is a graphite-like material with a van der Waals layered structure, which can be regarded as a nitrogen-substituted graphite framework through the sp^2 hybridization of carbon and nitrogen atoms. g-C_3N_4 possesses attractive properties such as suitable energy band structure, visible light absorption, and high chemical and thermal stability. g-C_3N_4 has been widely used in photocatalysis [51].

Hexagonal boron nitride (h-BN) and graphene have a highly similar crystal structure, which makes them share some common characteristics, such as extremely high elastic modulus, high-temperature stability, and atomically smooth surface. Like graphite, bulk h-BN also has a layered crystal structure. It consists of equal amounts of boron and nitrogen arranged in a hexagonal structure. Boron and nitrogen atoms are covalently bonded in each layer, and each layer is packed into bulk crystals by van der Waals forces. h-BN also has excellent characteristics such as wide band gap (5.9 eV), good insulation, chemical stability, and high thermal conductivity [52]. In addition to the materials mentioned above, the family of two-dimensional materials also includes metal-organic frameworks (MOFs), covalent organic frameworks (COFs), silicone, antimonene, black phosphorus carbides, and inorganic perovskites.

3 Electromagnetic meta-structures

3.1 The concept of meta-structures

Electromagnetic meta-structures refer to sub-wavelength or deep sub-wavelength artificial composites with a periodic structure that can attain various electromagnetic properties that are unattainable with natural materials [19, 20]. The term "Meta" can be interpreted as "super" or "beyond", referring to exceptional physical properties and phenomena that surpass those of natural or chemically synthesized materials, including negative dielectric constant, negative magnetic permeability, and negative refractive index [53–55]. In fact, electromagnetic meta-structures are an extremely general and broad concept, and depending on the context in which they are used, they can also be called metamaterials, metamorphic materials, left-handed materials, photonic crystals, and double-negative materials [56–58]. In general, the primary function of meta-structures is to modulate and customize the transmission properties of electromagnetic waves in space. Macroscopically, the electromagnetic properties of meta-structures emerge due to the periodic organization of specific electromagnetic responses. Microscopically, the structure of the periodic unit arrangement of meta-structures is akin to the arrangement of atoms and molecules in natural materials, with the unit structure of meta-structures equivalent to that of artificial atoms. This is because when the wavelength of the incident electromagnetic wave is much larger than the characteristic size of the metamaterial (meta-structures), the electric field component will cause the electrons inside the meta-structures to be shifted, resulting in a rise in the average electric field inside it, which will tend to zero when a large number of electrons are shifted, so that the metamaterial can be regarded as a homogeneous medium on a macroscopic level, which is precisely the source of the effective medium theory of meta-structures.

From an electromagnetic perspective, the response properties of any material to an electromagnetic field can be characterized by two physical parameters: permittivity ε and permeability μ [53]. By establishing a coordinate system with permittivity and permeability as the horizontal and vertical coordinates, respectively, all materials in dielectric space can be divided into four quadrants based on their positive and negative permittivity and permeability [53, 59], as shown in Figure 4. Through rational design, it is possible to make the equivalent permittivity and permeability of the meta-structure unit appear at any desired location in the dielectric space, thereby obtaining the desired exotic electromagnetic properties.

Based on the discussion above, metamaterials (or meta-structures) exhibit several fundamental characteristics. First, these materials possess artificially designed subwavelength or deep subwavelength structures, and these structural features originate from the concept of meta-structure design [60–62]. Second, meta-structures exhibit exceptional physical properties and phenomena when compared to natural materials [53–55]. Third, the extraordinary electromagnetic properties of meta-structures are mainly dependent on the artificially constructed structure, rather than the intrinsic properties of the material. This relationship can be explained through the effective medium theory [59, 60, 63]. The remarkable properties of meta-structures have made them an effective and widely accepted tool for modulating electromagnetic waves. This is the main reason why the combination of two-dimensional materials with meta-structures enables the achievement of multidimensional modulation of electromagnetic waves and several examples

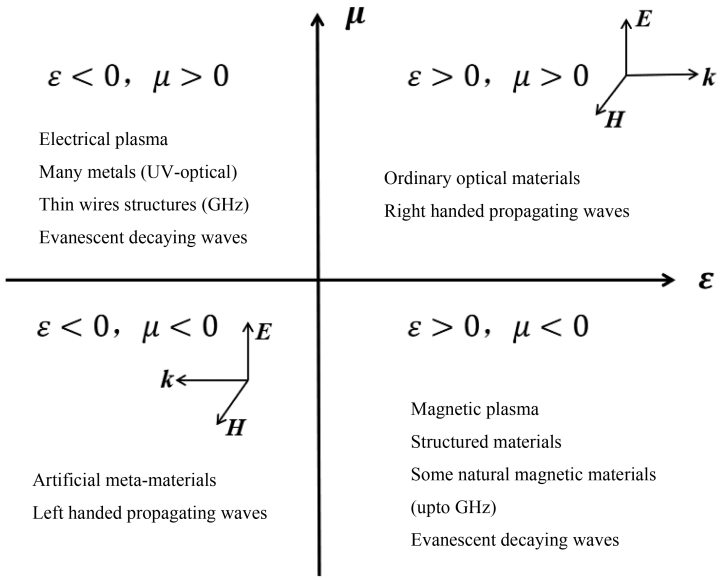

Figure 4 Schematic diagram of the electromagnetic medium space.

are presented in detail in the later contents to illustrate this point.

3.2 Mechanisms for achieving light field modulation in meta-structures

The mechanism by which meta-structures modulate light fields can be explored through the interaction of light fields with meta-structures. This interaction can be explained by the concept of resonance, which is the ability of meta-structures to enhance or suppress certain frequency components of electromagnetic waves due to the excitation of specific modes [54,55]. When the frequency of the incident electromagnetic wave is close to the resonant frequency of the meta-structure, the oscillation of electrons inside the meta-structure will be greatly enhanced, leading to a significant modulation of the transmitted electromagnetic wave [63–65]. The resonance effect of meta-structures is closely related to their structural features and design parameters, and can be flexibly adjusted by changing the structure and parameters of the meta-structures.

The meta-structures are structures with micro-nano dimensions, and at this scale, light fields often interact with these structures as evanescent waves [64]. The cases of Section 4 will demonstrate the role of surface plasmons, a unique form of the evanescent wave, in the modulation of electromagnetic waves. Surface plasmons are an independent electromagnetic mode that arises from the co-resonant oscillation of surface free charges [65,66]. The surface plasmon exhibits a variety of unique optical properties, including but not limited to selective absorption and scattering of light, and local field enhancement [67,68]. There are two types of surface plasmons: localized surface plasmon resonance (LSPR) and surface plasmon polariton (SPPs). Local surface plasmon resonance occurs when free electrons oscillate in metallic nanoparticles of a specific shape and size, while SPP is excited at the boundary between metallic films or two-dimensional materials and a medium and can propagate along the interface by conduction [65]. The SPPs excited in nanostructures are an electromagnetic mode that propagates along the interface of a metal and a dielectric material and in their ideal state, SPPs decay in a direction perpendicular to the interface, similar to the case of evanescent waves. Moreover, the wave vector of SPPs is usually higher than that of light waves at the same frequency, making it difficult to directly excite SPPs using plane light waves [69]. Therefore, SPPs are often excited through the introduction of special structures that satisfy the wave vector matching condition, such as prism coupling, grating coupling, and waveguide mode coupling [69–71]. In practice, however, we often encounter LSPR more frequently than SPPs, which are the ideal state of electromagnetic modes, because the micro- and nano-structures encountered are usually nanoparticles with specific shapes, such as nanospheres, nanorods, and nanowires.

In Figure 5, an illustration of a localized surface plasmon excited on a metal nanosphere is presented. When subjected to an external electric field, the free electrons situated on the surface of metal nanospheres exhibit reciprocating oscillations. These oscillations are restricted by boundary conditions to remain predominantly bound near the surface of the particles. This collective motion, known as localized surface

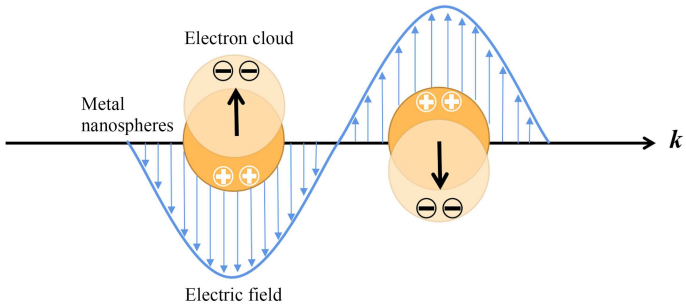

Figure 5 (Color online) Schematic representation of the situation when LSPs are excited on metal nanospheres.

plasmon, arises due to the interaction between the electromagnetic field and the free electron gas on the particle's surface. LSPR occurs when the frequency of the incident light wave matches the natural frequency of the plasmons and leads to a significant enhancement of the electromagnetic field both inside and outside the metal nanosphere [69–71]. The enhanced local fields within the nanoperiodic array structure indicate the successful excitation of specific electromagnetic modes that affect the incident light field, ultimately leading to anomalous absorption, transmission, and other optical phenomena [67, 68]. In fact, the mode of LSPR can be tailored by designing specific meta-structures that take into account the geometry, size, and material properties of micro- and nanostructures, providing a way to tune the incident light field.

The modulation of the incident light field (near-field region) has been previously discussed, whereas the modulation of the scattered light field (far-field region) will be addressed below. The source of the scattered light field is attributed to an electric or magnetic dipole, which functions as a secondary wave source and adheres to the Mie scattering theory [72, 73]. Micro-nano structures with specific features can generate dipoles in response to incident electromagnetic waves, similar to the phenomenon of LSPR. The resonance of the dipole generated by the micro-nano structure produces an electromagnetic field that gives rise to a scattered wave. The electromagnetic properties of the scattered wave are dictated by the array units of the micro-nano structure. As a result, this scattered wave can be utilized to manipulate the far-field radiation of electromagnetic waves. Therefore, the modulation of electromagnetic waves can be accomplished by designing meta-structures that can excite particular electromagnetic modes of surface plasmon or create specific dipole resonance scenarios.

3.3 Design and process preparation of meta-structures

The concept of inverse design, as applied to electromagnetic meta-structures, represents a novel approach to material design [61, 62]. This approach involves the rational design of periodic unit structures or overall structures that can overcome the limitations imposed by conventional laws of nature, thus enabling the realization of extraordinary electromagnetic functions tailored to specific needs. In contrast to the conventional approach of leveraging the properties of natural materials in the design of electromagnetic functional devices, meta-structures offer a more flexible and unconstrained design process. This design freedom, coupled with the extraordinary physical properties of meta-structures, has resulted in their growing significance for applications in the domains of imaging, detection, and communication [9–12]. Furthermore, the subwavelength design concept frequently serves as the foundation of the meta-structure design process.

In the inverse design of meta-structures, numerical calculations are frequently employed as a means of overcoming the complexity of their cell structures. This is due to the intricate relationships between edge values and the resulting electromagnetic field distributions that arise from the use of complex shapes. The solution of the resulting partial differential equations, which can be too complex to be solved directly, requires the assistance of a computer based on Maxwell's set of equations to analyze the response of the designed structure to the light field [74]. Three popular software programs that facilitate optical calculations are COMSOL Multiphysics, which leverages the finite element method, Ansys Lumerical FDTD, which employs the finite difference method in the time domain and CST Microwave Studio, which is based on time domain finite integration method [75–77]. These software programs represent valuable tools for the design of optical structures, owing to the convenience and ease they bring to the design process.

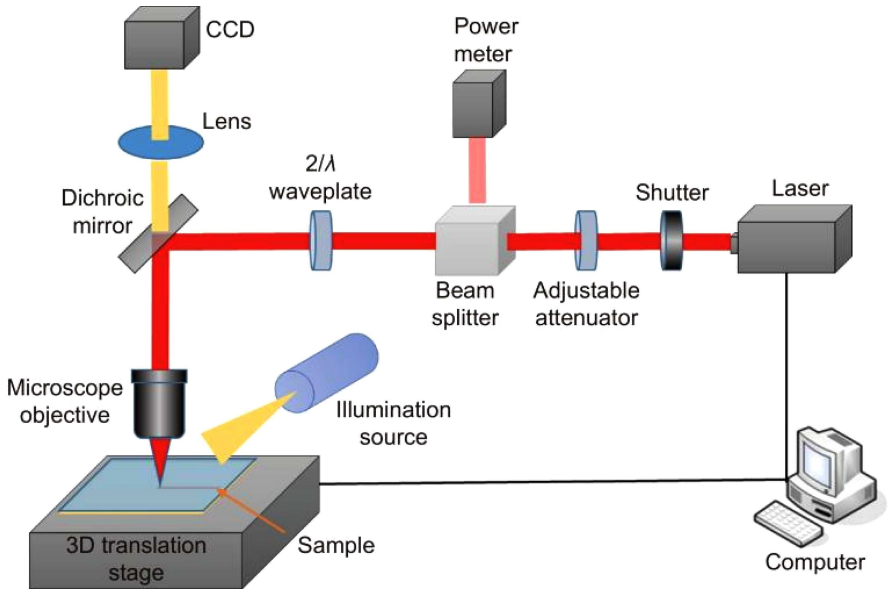

Figure 6 (Color online) Schematic diagram of a laser direct writing processing system [78] Copyright 2022 Editorial Office of Opto-Electronic Engineering, Institute of Optics and Electronics, Chinese Academy of Sciences.

Following the design of an optimal structure using simulation and computational software, a micro-nano process is employed to fabricate the structure and assess the actual modulation of the light field. The fabrication of micro and nano structures can be achieved using a range of techniques, such as photolithography, nanoimprinting, self-organization, focused ion beam, electron beam lithography, and laser direct writing [78–84]. Regardless of the specific fabrication process used, a layer-by-layer approach is typically employed. Notably, laser direct writing has emerged as a promising approach in recent years, owing to its potential for achieving high accuracy, high efficiency, and low cost. This technology employs a focused laser beam to selectively remove or modify the material from a substrate, enabling precise control over the shape and size of the structure being created. In this section, we provide a brief introduction to this method. The laser direct writing system consists of three key components: the laser source, the beam transmission system, and the motion control system, as illustrated in Figure 6. These components work in tandem to facilitate the flexible fabrication of fine micro and nano structures on a variety of materials, including both two-dimensional and three-dimensional substrates, with virtually limitless degrees of freedom [78]. The scale of processing achievable spans a range of orders of magnitude, from nanometers to millimeters. Moreover, the versatility of laser direct writing technology allows for the fabrication of complex 3D structures from a wide range of materials including metals, semiconductors, polymers, and ceramics, and can be integrated with other fabrication processes, such as photolithography and etching, to create even more complex structures [78,84]. In summary, laser direct writing technology represents a powerful tool for researchers and engineers working in the field of micro and nano fabrication. The technology's versatility, precision, and potential for integration with other fabrication processes make it a highly efficient and competitive method for the preparation of novel micro and nano structures and devices.

4 Several cases of multidimensional modulation of light fields by the combination of two-dimensional materials and meta-structures

4.1 Graphene-based

Plasmas describe collective oscillations of electrons. They play a fundamental role in the dynamic response of electronic systems and form the basis for the study of optical meta-structures. The 2D plasmon of massless electrons in graphene exhibits unusual behavior, enabling new tunable plasmonic meta-structures and potentially enabling optoelectronic applications in the terahertz frequency range.

Graphene and metasurfaces, as two special two-dimensional materials, can have unexpected effects when combined. The resonant frequency redshift of the Fano resonant metasurface can be achieved

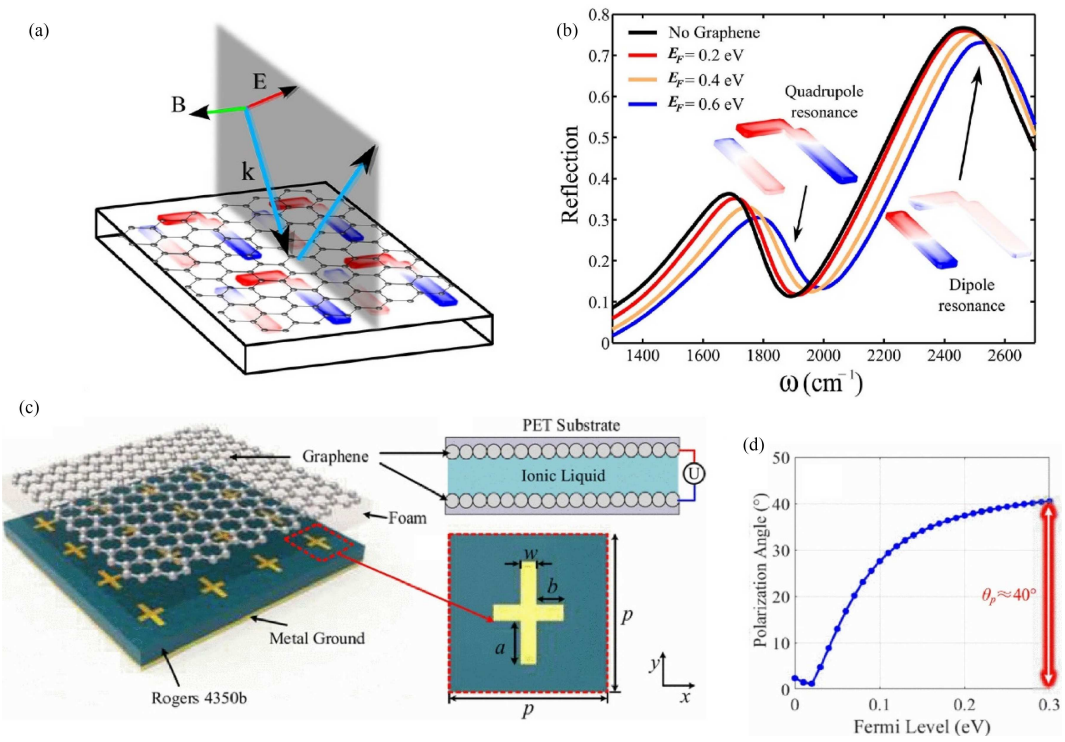

Figure 7 (Color online) Graphene metasurface. (a) Schematic diagram of plasmonic graphene metasurface [82]. (b) Reflection spectra at different Fermi energies. As the Fermi energy increases, the resonant frequency becomes larger [82] Copyright 2013 American Chemical Society. (c) Schematic diagram of the polarization-tunable graphene metasurface. The middle layer is a cross-shaped metal resonant layer, sandwiched by two layers of graphene, which can be changed by applying an applied voltage. The Fermi energy of graphene [85]. (d) The relationship between the polarization angle and the Fermi energy, as the Fermi energy increases from 0 to 0.3 eV, the polarization angle increases from 0° to 40° [85] Copyright 2021 IEEE.

by adding a protein monolayer on the metasurface, but the blueshift of the resonant frequency is very difficult for a long time. Mousavi et al. [82] placed chemically doped SLG on the Fano resonant mid-infrared metasurface, and used the plasmonic response of graphene in the mid-infrared band to make graphene and the metasurface inductively coupled to achieve Blueshift reconcilability. SLG exhibits a strong plasmonic response and negligible loss, and its conductivity has a large dependence on the Fermi energy, which can be controlled by controlling chemical doping and electrostatic gates, with a large adjustment space. Figure 7(a) is a schematic diagram of a single layer of graphene covered on a metasurface [82]. Figure 7(b) is the reflection spectrum after the electromagnetic wave is incident. It can be seen that the addition of SLG makes the overall resonance blue shift, and the magnitude of the blue shift can be controlled by the size of the Fermi energy.

The polarization of electromagnetic waves is a very important state of electromagnetic waves, and it is very meaningful to freely control the polarization state of electromagnetic waves. The graphene metasurface proposed by Zhang et al. [85] can control the microwave's polarization state of electromagnetic waves. One of the reasons why graphene can be used as a candidate material for metasurfaces is because it can change the Fermi energy through chemical and electrostatic doping to achieve dynamic regulation of surface impedance in a broadband band [86]. Figure 7(c) shows a schematic diagram of the graphene metasurface, with graphene on the upper and lower sides sandwiching the copper layer of the cross resonator. A voltage bias device is added between the two graphene layers to achieve electrostatic doping and dynamically adjust the Fermi energy of graphene [87]. Figure 7(d) shows the polarization angles corresponding to different Fermi energies. It can be seen that as the Fermi energy level increases from 0 to 0.3 eV, the polarization angle can increase from 0° to 40°.

The combination of graphene and metasurface can also be applied to photodetection. Near-infrared narrowband photodetection has very important application value, but generally relies on additional filters and spectrometers, which is not conducive to the miniaturization of chip integration [88,89]. Polarization-sensitive narrowband infrared photodetection can be realized by optical Tamm state engineering [88]. Optical Tamm states are found in one-dimensional multilayer photonic structures, which can confine

electromagnetic waves at interfaces. The Tamm plasma structure consists of a distributed Bragg reflector (DBR), a dielectric spacer, and a metal film. DBR is a periodic structure, and each period is composed of three layers of thin films. Above DBR is a dielectric thin film and a metal layer. Due to the weak van der Waals interlayer interactions, Bi-layer graphene was mechanically exfoliated on the prepared DBR by scotch tape. Electrodes were then fabricated using standard photolithographic processes of electron beam lithography and thermal evaporation, followed by spin-coating of poly methyl meth acrylate (PMMA) on the device surface and forming a window in the center of the graphene channel, depositing a dielectric layer and a gold film/gate. As the thickness of the dielectric layer changes, its absorption peak also changes. The hybrid device exhibits a high responsivity of 187 mA/W at 1550 nm, which is nearly 100 times higher than that based on bare graphene. If the metal film on the upper layer is replaced by a metal grating, there will be different responses to incidents in the x-direction and y-direction. For two orthogonal polarizations, the grating-based device exhibits a high dichroic ratio of 4.6 at a wavelength of 1300 nm and a high dichroic ratio of 2.5 at a wavelength of 1500 nm. Using a similar structure, the photoelectric detection device can achieve angle selection in the near-infrared region and wavelength selection in the visible region. SLG grown on copper foil using chemical vapor deposition technique was transferred using wet chemical methods [89].

4.2 TMDS-based

Monolayer MoS_2 has two unequal valleys in the Brillouin zone, and each valley can couple polarized photons with a specific degree of rotation. We have mentioned before that the valley fluorescence signal is weak at room temperature and the scattering performance between K and K$'$ valleys is equivalent. Here we discuss the modulation of the valley-polarized PL of MoS_2 through the near-field interaction of plasmonic chiral metasurfaces.

Li et al. [90] achieved manipulation of MoS_2 valley-polarized PL in metasurface heterostructures using a metal-dielectric-metal plasmonic chiral structure. The schematic diagram and scanning electron microscopy (SEM) image of the MoS_2 metasurface are shown in Figures 8(a) and (b). The MoS_2 layer is sandwiched between the metasurface and the gold film. The MoS_2 film appears triangular because it is a 2H crystal phase. Experiments show that compared with single-layer MoS_2 films, the PL intensity and spectral absorption of MoS_2 metasurfaces are significantly improved. Figure 8 shows the polarized PL of MoS_2 thin film and MoS_2 metasurface excited by circularly polarized light, Figures 8(c) and (d) are the polarization PL of MoS_2 film and MoS_2 metasurface under σ-light excitation, and Figure 8(e) is the corresponding degree of valley polarization (DVP). The DVP is a parameter characterizing the purity of valley-polarized PL, expressed as $p = (I_- - I_+)/(I_- + I_+)$. I_- and I_+ experimentally measured left-handed and right-handed light. It can be found that due to the existence of the metasurface, the intensity of the electromagnetic near field is enhanced, which makes the intensity of σ-PL increase. The DVP of the metasurface reaches 43%, much larger than 25% of the film. Figures 8(f)–(h) are the corresponding images under $\sigma+$ light excitation, the PL is also enhanced, but the DVP of the MoS_2 metasurface is suppressed to 20%, while the DVP of single-layer showed completely consistent results. All the above results indicate that the valley-polarized PL of the metasurface can be modulated under the near-field interaction of circular polarization. The motivation is that the chiral field induced by the plasmonic chiral metasurface couples with the pseudo-spin valley of, thus facilitating the exciton absorption and emission.

4.3 Mxene-based

Zhou et al. [91] used $Ti_3C_2T_x$ and black phosphorus to construct a new type of metasurface to achieve tunable light field enhancement. The transmission spectrum and electric field light intensity of the metasurface were studied using the finite difference time domain simulation method [75]. Figure 9(a) shows a schematic diagram of the structure of the composite metasurface, in which MXene and black phosphorus are periodically arranged on a glass substrate. Figure 9(b) gives the corresponding spectrum and field intensity distribution when linearly polarized light is incident along the z direction. The red line, black line, and blue line in the spectrogram represent the spectrum of only black phosphorus, MXene, and the combination of the two, respectively. A drop in transmission can be clearly seen at 9.75 and 32.54 THz, corresponding to the plasmons on the respective surfaces of black phosphorus and MXene, respectively. For the metasurface formed by the combination of the two, the respective plasmons of black phosphorus and MXene are coupled at the interface, and the spectrum presents the characteristics of Fano resonance, with a peak at 25.34 THz. In addition, the study also found that the spectral and field

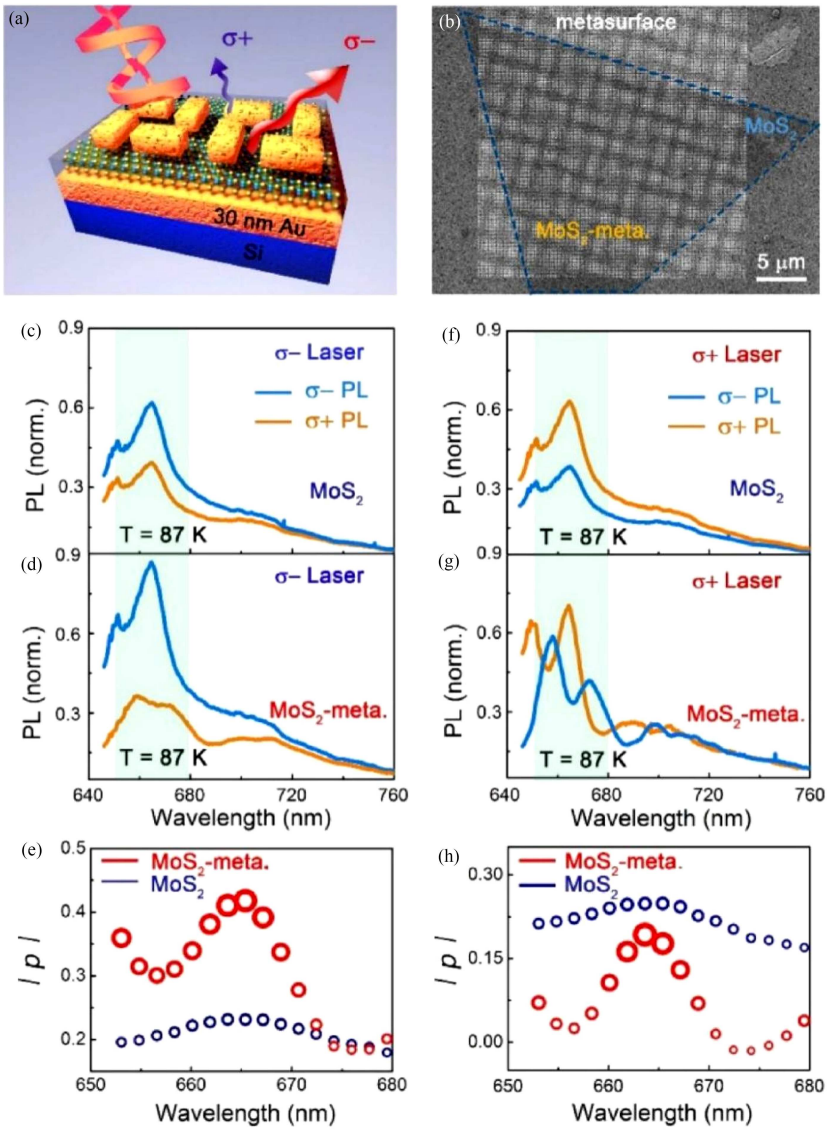

Figure 8 (Color online) (a) Schematic diagram and (b) SEM image of TMDS metasurface, the metasurface is a metal-dielectric-metal structure, and the MoS_2 thin film is triangular [90]; (c) PL intensity of MoS_2 film and (d) PL intensity of MoS_2 metasurface after $\sigma-$ incident [90]; (e) valley polarization degree of MoS_2 film and MoS_2 metasurface; (f) PL intensity of MoS_2 film and (g) PL intensity of MoS_2 metasurface after $\sigma+$ incident [90]; (h) valley polarization degree of MoS_2 film and MoS_2 metasurface [90] Copyright 2018 WILEY-VCH Verlag GmbH & Co. KGaA, Weinheim.

enhancement ratios have a strong dependence on the structural parameters and polarization directions. For example, when the width of the black phosphorus increases from 250 to 350 nm, the plasmon coupling at the interface between the black phosphorus and MXene weakens, and the Fano response gradually disappears. When the polarization direction of the incident linearly polarized light increases from 0° to 90°, the Fano response also gradually disappears due to the selectivity of the metasurface structure on the light polarization [91].

Li et al. [92] prepared an electrically driven active VO_2/MXene metasurface that can regulate electromagnetic waves in the terahertz band. The schematic diagram and SEM image of the metasurface are shown in Figure 10(a). Figures 10(b)–(d) show the spectral response of the metasurface. Under electric field stimulation, the transmittance at 0.43 THz is reduced from 0.91 to 0.13, and its trigger power is much lower than other active devices. The modulation depth is defined as $(T_2 - T_1)/T_1$, where T_2 and T_1 are the transmittance with and without modulation, respectively. The modulation depth of the metasurface here reaches 85.7%, which is a great improvement compared to 62.9% of the single VO_2 film as shown in Figures 10(b) and (c). The picture shows that after the metasurface is heated, the phase transition of VO_2 causes the transmittance to drop to 0 in the whole band. Figure 10(e) is the response speed of the

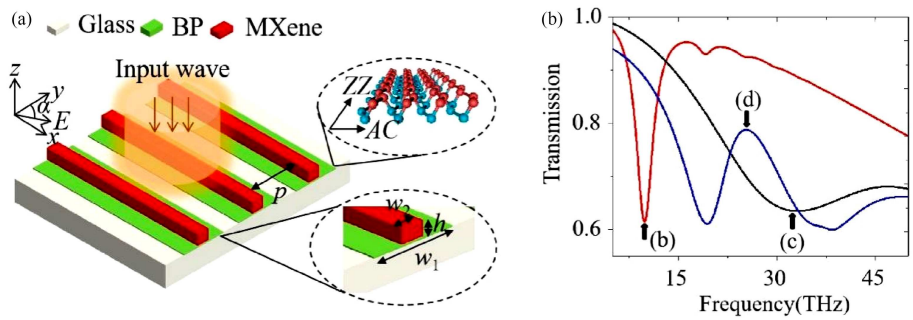

Figure 9 (Color online) (a) Black phosphorus and $Ti_3C_2T_x$ composite metasurface, $Ti_3C_2T_x$ is on the black phosphorus, and the black phosphorus is arranged periodically on the base [91]; (b) $Ti_3C_2T_x$ transmission spectra of metasurfaces exhibiting Fano resonances [91] Copyright 2022 by the authors.

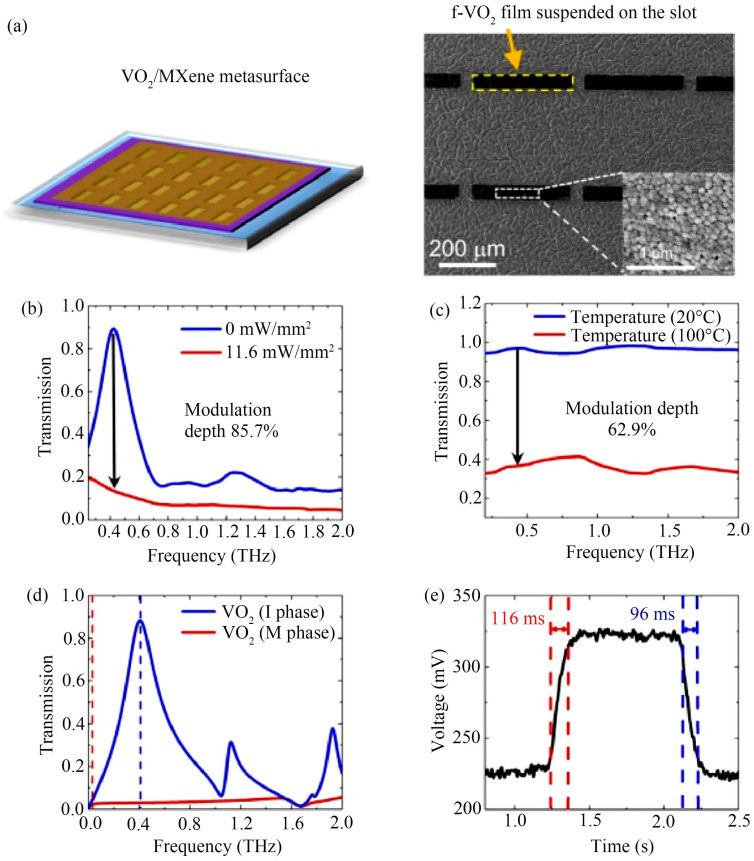

Figure 10 (Color online) (a) Schematic diagram and SEM image of VO_2/MXene metasurface [92]; (b) transmission spectrum with and without electric field of 11.6 mW/mm^2; (c) transmission spectrum at 20° and 100°; (d) two transmission spectra of the metasurface in different VO_2 phases; (e) response time of the active metasurface [92] Copyright 2022 AIP Publishing.

metasurface. In addition to amplitude regulation, the polarization extinction ratio of the metasurface reaches 14.1 dB. The aforementioned properties indicate that the metasurface can be used as a terahertz polarizer and amplitude modulator, and has practical application value in imaging systems.

4.4 Some others

Chirality is of great significance in analytical chemistry, spectroscopy, optics, and other fields. In the field of optics, chiral objects can exhibit different optical responses when interacting with circularly polarized light of different polarities. The chiral response of natural chiral materials is generally weak, while that of chiral meta-structures is much larger [93]. In particular, plasmonic metal nanostructures are widely used in the design of chiral meta-structures. As an in-plane anisotropic material, black phosphorus can achieve extrinsic chirality under oblique incident light, but the response is not strong [94]. Extrinsic

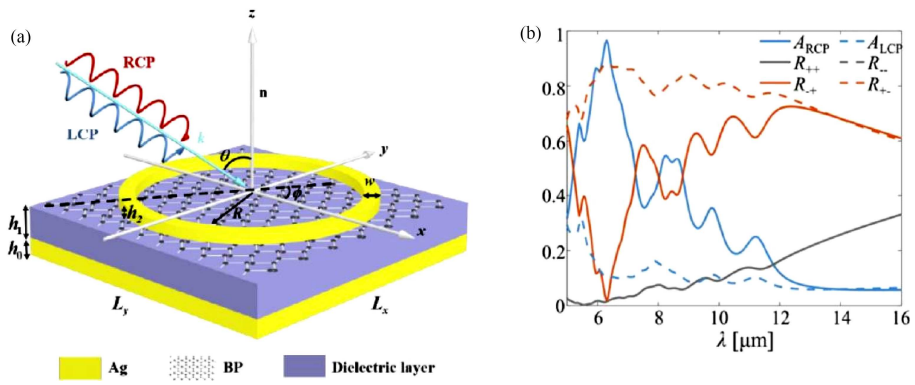

Figure 11 (Color online) (a) The black phosphorus super surface schematic diagram, the bottom layer is silver reflex layer and electron substrate base, the middle is black phosphorus, and the above is the absorption and reflection of the silver ring. (b) Electromagnetic waves. Different polarized light responses are different [95] Copyright 2022 Optica Publishing Group under the Terms of the Optica Open Access Publishing Agreement.

chirality means that when a light wave is obliquely incident on an achiral metamaterial, the planar chiral structure and the incident polarized wave form an achiral arrangement, resulting in a chiral response. Zeng et al. [95] used the black phosphorus metasurface to achieve a huge two-dimensional extrinsic chiral response in the infrared band. Figure 11(a) is a schematic diagram of the black phosphorus metasurface, which mainly consists of four layers, from top to bottom are the silver ring array, a single layer of black phosphorus, a dielectric layer, and a silver reflective surface. When the electromagnetic wave is obliquely incident, Figure 11(b) shows the corresponding optical response when the incident angle is $\theta = 80°$, $\varphi = 49°$, and A_{RCP}, R_{++}, R_{-+} respectively represent the absorption of right-handed light, right-handed light is converted to right-handed light, right-handed light is converted to left-handed light, and A_{RCP}, R_{++}, R_{-+} represent the corresponding responses to left-handed light. It can be seen that there are many peaks in the absorption curve, part of which is caused by the coupling between the black phosphorus surface plasmon mode and the localized surface plasmon mode between adjacent metal rings, and partly due to the wave vector provided by the silver ring array excited black phosphorus plasmons with different grating orders. In fact, this kind of metasurface has great coordination. The oblique incident angle of light waves, the structural parameters of the metasurface, and the doping concentration of the single-layer black phosphorus all affect the extrinsic chiral response of the achiral metasurface. For example, when the dopant concentration increases, the conductivity of the single-layer black phosphorus changes, and the spectrum will blue shift; the spacer has a great influence on the wavelength of the Fabry-Perot resonance of the black phosphorus silver reflective surface. Therefore, the chiral response of this tunable achiral black phosphorus metasurface is expected to be applied to circular polarizers and polarization modulators in the infrared band. In addition to the modulation of the polarization of light, the optical angular momentum is also a very important parameter. Direct measurements of optical angular momentum are required, as opposed to measurements achieved using interference and diffraction properties. The photodetector based on Type-II Weyl semimetal TaIrTe4 with designed electrode geometry can directly measure the topological charge of OAM through OPGE at 4 μm [96].

5 Conclusion and outlook

The combination of two-dimensional materials and metasurfaces can create a new promising field, especially the multi-dimensional modulation of the light field. In this article, we first introduced the properties of two-dimensional materials and several typical representatives, such as graphene, TMDS, MXene, and black phosphorus. Then the concept, principle, design, and preparation of the metasurface are introduced. Finally, several examples of the combination of 2D materials and metamaterials are given.

The combination of 2D materials and metasurfaces has many advantages. First, in the past, most metamaterials were designed with dielectrics and metals as raw materials, and two-dimensional materials, as a large category, can greatly expand the range of material choices. Second, two-dimensional materials have good coordination, and the properties of materials can be changed through doping concentration, etc., which is of great significance for the realization of multifunctional devices. Third, since two-dimensional materials and metasurfaces are only two-dimensional, the combination of the two will

not change the advantages of small size, which has great practical application value. There are also many difficulties and challenges in the combination of two-dimensional materials and metasurfaces. On the one hand, for ultra-thin two-dimensional nanomaterials, the current output, quality, and productivity are far from industrialization, and the understanding of the growth mechanism and performance of two-dimensional materials is not simple. In order to apply two-dimensional materials to a practical range, the prepared ultra-thin two-dimensional materials also need to have relatively good physical and chemical stability, which cannot be achieved at present. Although metasurfaces have shown powerful functions in regulating electromagnetic waves, they have high requirements on materials. In metasurface-related devices, the dispersion and loss of materials often degrade the performance of the device, and the process of designing metasurfaces is also a complicated process. The combination of two-dimensional materials and metasurfaces can indeed achieve many expected phenomena, but this puts forward higher requirements for the preparation and design of two-dimensional materials.

Here, we make a certain outlook on the combination of metamaterials and 2D materials. As the preparation methods of two-dimensional materials become more perfect and the understanding of the properties and mechanisms of two-dimensional materials continues to deepen, it is entirely possible to prepare stable two-dimensional materials. The design of metasurface multifunctional devices often requires constant adjustment of parameters to achieve the goal, but this process often requires huge resources. With the rise of artificial intelligence, the design of metasurfaces may be handed over to artificial intelligence. Under the combination of metasurfaces and two-dimensional materials, electromagnetic devices are bound to usher in an explosion in the future.

Acknowledgements This work was supported by National Key Research and Development Program of China (Grant Nos. 2019YFA0210203, 2020YFA0211300), National Natural Science Foundation of China (Grant Nos. 62225501, 12027807), and High-performance Computing Platform of Peking University.

References

1 Xu X, Wang C, Shou W, et al. Physical realization of elastic cloaking with a polar material. Phys Rev Lett, 2020, 124: 114301
2 Zhang L P, Zhang H C, Tang M, et al. Integrated multi-scheme digital modulations of spoof surface plasmon polaritons. Sci China Inf Sci, 2020, 63: 202302
3 Li J, Li J, Yue Z, et al. Structured vector field manipulation of terahertz wave along the propagation direction based on dielectric metasurfaces. Laser Photon Rev, 2022, 16: 2200325
4 Yu N, Capasso F. Flat optics with designer metasurfaces. Nat Mater, 2014, 13: 139–150
5 Zhang Y, Zhang F, Du B, et al. Au/MXene based ultrafast all-optical switching. Front Phys, 2023, 18: 33301
6 Gurses V. Enhancing spatiotemporal light modulators. Nat Photon, 2022, 16: 818–820
7 Pan H Y, Chen X, Xia X L. A review on the evolvement of optical-frequency filtering in photonic devices in 2016–2021. Renew Sustain Energy Rev, 2022, 161: 112361
8 Wachter S, Polyushkin D K, Bethge O, et al. A microprocessor based on a two-dimensional semiconductor. Nat Commun, 2017, 8: 14948
9 Winzer P J. Scaling optical fiber networks: challenges and solutions. Opt Photon News, 2015, 26: 28
10 Long T, Liang Z N, Liu Q H. Advanced technology of high-resolution radar: target detection, tracking, imaging, and recognition. Sci China Inf Sci, 2019, 62: 40301
11 Zheng D, Wen Y, Xu X, et al. Metamaterial grating for colorimetric chemical sensing applications. Mater Today Phys, 2023, 33: 101056
12 Balci O, Kakenov N, Karademir E, et al. Electrically switchable metadevices via graphene. Sci Adv, 2018, 4:
13 Chen Y, Wang X, Wang P, et al. Optoelectronic properties of few-layer MoS_2 FET gated by ferroelectric relaxor polymer. ACS Appl Mater Interfaces, 2016, 8: 32083–32088
14 Long G, Maryenko D, Shen J, et al. Achieving ultrahigh carrier mobility in two-dimensional hole gas of black phosphorus. Nano Lett, 2016, 16: 7768–7773
15 Zhou J, Sun Q, Wang Q, et al. High-temperature superconductivity in heavily N- or B-doped graphene. Phys Rev B, 2015, 92: 064505
16 Tarnopolsky G, Kruchkov A J, Vishwanath A. Origin of magic angles in twisted bilayer graphene. Phys Rev Lett, 2019, 122: 106405
17 Jana M K, Song R, Liu H, et al. Organic-to-inorganic structural chirality transfer in a 2D hybrid perovskite and impact on Rashba-Dresselhaus spin-orbit coupling. Nat Commun, 2020, 11: 4699
18 Smith D R, Pendry J B, Wiltshire M C K. Metamaterials and negative refractive index. Science, 2004, 305: 788–792
19 Jin Y, Wang W, Khelif A, et al. Elastic metasurfaces for deep and robust subwavelength focusing and imaging. Phys Rev Appl, 2021, 15: 024005
20 Zhong Y L, Tian Z, Simon G P, et al. Scalable production of graphene via wet chemistry: progress and challenges. Mater Today, 2015, 18: 73–78
21 Jiang H B, Zhang Y L, Liu Y, et al. Bioinspired few-layer graphene prepared by chemical vapor deposition on femtosecond laser-structured Cu foil. Laser Photon Rev, 2016, 10: 441–450
22 Chang C, Chen W, Chen Y, et al. Recent progress on two-dimensional materials. Acta Phys Chim Sin, 2021, 0: 2108017
23 Ganz E, Sattler K, Clarke J. Scanning tunneling microscopy of the local atomic structure of two-dimensional gold and silver islands on graphite. Phys Rev Lett, 1988, 60: 1856–1859
24 Chen Y, Fan Z, Zhang Z, et al. Two-dimensional metal nanomaterials: synthesis, properties, and applications. Chem Rev, 2018, 118: 6409–6455
25 Coleman J N, Lotya M, O'Neill A, et al. Two-dimensional nanosheets produced by liquid exfoliation of layered materials. Science, 2011, 331: 568–571

26 Cai Z, Liu B, Zou X, et al. Chemical vapor deposition growth and applications of two-dimensional materials and their heterostructures. Chem Rev, 2018, 118: 6091–6133
27 Zhang H. Introduction: 2D materials chemistry. Chem Rev, 2018, 118: 6089–6090
28 Varghese N, Mogera U, Govindaraj A, et al. Binding of DNA nucleobases and nucleosides with graphene. ChemPhysChem, 2009, 10: 206–210
29 Novoselov K S, Geim A K, Morozov S V, et al. Electric field effect in atomically thin carbon films. Science, 2004, 306: 666–669
30 Liu F, Navaraj W T, Yogeswaran N, et al. van der Waals contact engineering of graphene field-effect transistors for large-area flexible electronics. ACS Nano, 2019, 13: 3257–3268
31 Papageorgiou D G, Kinloch I A, Young R J. Mechanical properties of graphene and graphene-based nanocomposites. Prog Mater Sci, 2017, 90: 75–127
32 Yildiz G, Bolton-Warberg M, Awaja F. Graphene and graphene oxide for bio-sensing: general properties and the effects of graphene ripples. Acta Biomater, 2021, 131: 62–79
33 Olabi A G, Abdelkareem M A, Wilberforce T, et al. Application of graphene in energy storage device — a review. Renew Sustain Energy Rev, 2021, 135: 110026
34 Du J, Fu G, Xu X, et al. 3D printed graphene-based metamaterials: guesting multi-functionality in one gain. Small, 2023. doi: 10.1002/smll.202207833
35 Perruisseau-Carrier J. Graphene for antenna applications: opportunities and challenges from microwaves to THz. In: Proceedings of Antennas and Propagation Conference, 2013
36 Fan Y, Shen N, Zhang F, et al. Two-dimensional optics: graphene plasmonics: a platform for 2D optics (Advanced Optical Materials 3/2019). Adv Opt Mater, 2019, 7: 1970009
37 Fei Z, Rodin A S, Andreev G O, et al. Gate-tuning of graphene plasmons revealed by infrared nano-imaging. Nature, 2012, 487: 82–85
38 Cyrus S, Biabanifard S. Graphene-based THz absorber: adjustability via multiple gate biasing. Heliyon, 2021, 7: e07633
39 Brar V W, Jang M S, Sherrott M, et al. Highly confined tunable mid-infrared plasmonics in graphene nanoresonators. Nano Lett, 2013, 13: 2541–2547
40 Yan H, Li X, Chandra B, et al. Tunable infrared plasmonic devices using graphene/insulator stacks. Nat Nanotech, 2012, 7: 330–334
41 Ju L, Geng B, Horng J, et al. Graphene plasmonics for tunable terahertz metamaterials. Nat Nanotech, 2011, 6: 630–634
42 Zhao B, Shen D, Zhang Z, et al. 2D metallic transition-metal dichalcogenides: structures, synthesis, properties, and applications. Adv Funct Mater, 2021, 31: 2105132
43 Mupparapu R, Bucher T, Staude I. Integration of two-dimensional transition metal dichalcogenides with Mie-resonant dielectric nanostructures. Adv Phys-X, 2020, 5: 1734083
44 Deng M, Wang X, Chen J, et al. Plasmonic modulation of valleytronic emission in two-dimensional transition metal dichalcogenides. Adv Funct Mater, 2021, 31: 2010234
45 Tang Q, Zhou Z, Shen P. Are MXenes promising anode materials for Li ion batteries? Computational studies on electronic properties and Li storage capability of Ti_3C_2 and $Ti_3C_2X_2$ (X = F, OH) monolayer. J Am Chem Soc, 2012, 134: 16909–16916
46 Hope M A, Forse A C, Griffith K J, et al. NMR reveals the surface functionalisation of Ti_3C_2 MXene. Phys Chem Chem Phys, 2016, 18: 5099–5102
47 Wang H, Wu Y, Zhang J, et al. Enhancement of the electrical properties of MXene Ti_3C_2 nanosheets by post-treatments of alkalization and calcination. Mater Lett, 2015, 160: 537–540
48 Cao M, Shu J, Wang X, et al. Electronic structure and electromagnetic properties for 2D electromagnetic functional materials in gigahertz frequency. Annalen Der Physik, 2019, 531: 1800390
49 Yang S, Zhang K, Ricciardulli A G, et al. A delamination strategy for thinly layered defect-free high-mobility black phosphorus flakes. Angew Chem, 2018, 130: 4767–4771
50 Correas-Serrano D, Gomez-Diaz J S, Alú A. Mid-infrared plasmon canalization over black phosphorus metasurfaces. In: Proceedings of IEEE International Symposium on Antennas and Propagation and USNC/URSI National Radio Science Meeting, 2017. 1069–1070
51 Ong W J, Tan L L, Ng Y H, et al. Graphitic carbon nitride (g-C_3N_4)-based photocatalysts for artificial photosynthesis and environmental remediation: are we a step closer to achieving sustainability? Chem Rev, 2016, 116: 7159–7329
52 Tan C, Cao X, Wu X J, et al. Recent advances in ultrathin two-dimensional nanomaterials. Chem Rev, 2017, 117: 6225–6331
53 Jahani S, Jacob Z. All-dielectric metamaterials. Nat Nanotech, 2016, 11: 23–36
54 Estep N A, Askarpour A N, Alu A. Experimental demonstration of negative-index propagation in a rectangular waveguide loaded with complementary split-ring resonators. Antennas Wirel Propag Lett, 2015, 14: 119–122
55 Guo C, Luo Y. Light people: prof. Sir John Pendry, father of metamaterials, spoke about the future of meta. Light Sci Appl, 2023, 12: 45
56 Zhang D, Zheng H, Ma X, et al. On-demand circularly polarized room-temperature phosphorescence in chiral nematic nanoporous silica films. Adv Opt Mater, 2022, 10: 2102015
57 Liu J W, Shi F L, He X T, et al. Valley photonic crystals. Adv Phys-X, 2021, 6: 1905546
58 Zhang T, Zheng C Q, Chen Z N, et al. Negative reflection and negative refraction in biaxial van der Waals materials. Nano Lett, 2022, 22: 5607–5614
59 Silveirinha M, Engheta N. Design of matched zero-index metamaterials using nonmagnetic inclusions in epsilon-near-zero media. Phys Rev B, 2007, 75: 075119
60 Valentine J, Zhang S, Zentgraf T, et al. Three-dimensional optical metamaterial with a negative refractive index. Nature, 2008, 455: 376–379
61 Zeng Q, Duan S, Zhao Z, et al. Inverse design of energy-absorbing metamaterials by topology optimization. Adv Sci, 2023, 10: 2204977
62 Shelby R A, Smith D R, Schultz S. Experimental verification of a negative index of refraction. Science, 2001, 292: 77–79
63 Liu Y C, Wang G P, Zhang S. A nonlocal effective medium description of topological Weyl metamaterials. Laser Photon Rev, 2021, 15: 2100129
64 Hibbins A P, Evans B R, Sambles J R. Experimental verification of designer surface plasmons. Science, 2005, 308: 670–672
65 Rawashdeh A, Wildenborg A, Liu E, et al. High-quality surface plasmon polaritons in large-area sodium nanostructures. Nano Lett, 2023, 23: 469–475
66 Maier S A, Andrews S R, Martín-Moreno L, et al. Terahertz surface plasmon-polariton propagation and focusing on periodically corrugated metal wires. Phys Rev Lett, 2006, 97: 176805

67 Shen X, Jun Cui T. Planar plasmonic metamaterial on a thin film with nearly zero thickness. Appl Phys Lett, 2013, 102: 211909
68 Zhang H C, Liu S, Shen X, et al. Broadband amplification of spoof surface plasmon polaritons at microwave frequencies. Laser Photon Rev, 2015, 9: 83–90
69 Elbanna A, Jiang H, Fu Q, et al. 2D material infrared photonics and plasmonics. ACS Nano, 2023, 17: 4134–4179
70 Raman A, Shin W, Fan S. Upper bound on the modal material loss rate in plasmonic and metamaterial systems. Phys Rev Lett, 2013, 110: 183901
71 Drachev V P, Chettiar U K, Kildishev A V, et al. The Ag dielectric function in plasmonic metamaterials. Opt Express, 2008, 16: 1186–1195
72 Yan J, Yang X, Liu X, et al. Van der Waals heterostructures with built-in Mie resonances for polarization-sensitive photodetection. Adv Sci, 2023, 10: 2207022
73 Adachi M, Sugimoto H, Nishimura Y, et al. Fluorophore-decorated Mie resonant silicon nanosphere for scattering/fluorescence dual-mode imaging. Small, 2023, 19: 2207318
74 Zhao S, Wei G W. High-order FDTD methods via derivative matching for Maxwell's equations with material interfaces. J Comput Phys, 2004, 200: 60–103
75 Oskooi A F, Roundy D, Ibanescu M, et al. Meep: a flexible free-software package for electromagnetic simulations by the FDTD method. Comput Phys Commun, 2010, 181: 687–702
76 Putrino G, Keating A, Martyniuk M, et al. Model and analysis of a high sensitivity resonant optical read-out approach suitable for cantilever sensor arrays. J Lightwave Technol, 2012, 30: 1863–1868
77 Wang J, Wu Z, Xing Y, et al. Multi-scale design of ultra-broadband microwave metamaterial absorber based on hollow carbon/MXene/Mo_2C microtube. Small, 2023, 19:
78 Zhou W P, Bai S, Xie Z W, et al. Research progress of laser direct writing fabrication of metal and carbon micro/nano structures and devices. Opto-Electron Eng, 2022, 49: 210330
79 Kim J, Kim W, Oh D K, et al. One-step printable platform for high-efficiency metasurfaces down to the deep-ultraviolet region. Light Sci Appl, 2023, 12: 68
80 Wang D, Xu T, Zhang M, et al. A novel layered WO_3 derived from an ion etching engineering for ultrafast proton storage in frozen electrolyte. Adv Funct Mater, 2023, 33: 2211491
81 Sundaramurthy A, Schuck P J, Conley N R, et al. Toward nanometer-scale optical photolithography: utilizing the near-field of bowtie optical nanoantennas. Nano Lett, 2006, 6: 355–360
82 Mousavi S H, Kholmanov I, Alici K B, et al. Inductive tuning of fano-resonant metasurfaces using plasmonic response of graphene in the mid-infrared. Nano Lett, 2013, 13: 1111–1117
83 Liu Y, Qu Y, Liu Y, et al. Direct-writing of 2D diodes by focused ion beams. Adv Funct Mater, 2021, 31: 2102708
84 Bruchhaus L, Mazarov P, Bischoff L, et al. Comparison of technologies for nano device prototyping with a special focus on ion beams: a review. Appl Phys Rev, 2017, 4: 011302
85 Zhang J, Zhu W. Dynamic polarization manipulation in graphene-based metasurface. In: Proceedings of IEEE MTT-S International Microwave Workshop Series on Advanced Materials and Processes for RF and THz Applications (IMWS-AMP), 2021. 290–292
86 Fan C, Wu B, Hu Y, et al. Millimeter-wave pattern reconfigurable vivaldi antenna using tunable resistor based on graphene. IEEE Trans Antennas Propagat, 2019, 68: 4939–4943
87 Zhang J, Wei X, Rukhlenko I D, et al. Electrically tunable metasurface with independent frequency and amplitude modulations. ACS Photon, 2019, 7: 265–271
88 Yu Y, Zhong F, Chu Q, et al. Polarization-sensitive narrowband infrared photodetection triggered by optical Tamm state engineering. Opt Express, 2023, 31: 8797–8804
89 Huang C H, Wu C H, Bikbaev R G, et al. Wavelength- and angle-selective photodetectors enabled by graphene hot electrons with Tamm plasmon polaritons. Nanomaterials, 2023, 13: 693
90 Li Z, Liu C, Rong X, et al. Tailoring MoS_2 valley-polarized photoluminescence with super chiral near-field. Adv Mater, 2018, 30: 1801908
91 Zhou Y, Li L, He Z, et al. Field enhancement for the composite MXene/black phosphorus-based metasurface. Nanomaterials, 2022, 12: 3155
92 Li Y, Ma H, Wang Y, et al. Electrically driven active VO_2/MXene metasurface for the terahertz modulation. Appl Phys Lett, 2022, 121: 241902
93 Wang Z, Cheng F, Winsor T, et al. Optical chiral metamaterials: a review of the fundamentals, fabrication methods and applications. Nanotechnology, 2016, 27: 412001
94 Hong Q, Xu W, Zhang J, et al. Optical activity in monolayer black phosphorus due to extrinsic chirality. Opt Lett, 2019, 44: 1774–1777
95 Zeng Y, Xu J, Xiao W, et al. Giant 2D-chiroptical response in an achiral metasurface integrated with black phosphorus. Opt Express, 2022, 30: 8266–8274
96 Lai J, Ma J, Fan Z, et al. Direct light orbital angular momentum detection in mid-infrared based on the type-II Weyl semimetal $TaIrTe_4$. Adv Mater, 2022, 34: 2201229